World Academy of Science, Engineering and Technology
International Journal of Computer and Information Engineering
Vol:1, No:12, 2007

# Evaluation of Mixed-Mode Stress Intensity Factor by Digital Image Correlation and Intelligent Hybrid Method

K. Machida, and H. Yamada



***Abstract*—**Displacement measurement was conducted on compact normal and shear specimens made of acrylic homogeneous material subjected to mixed-mode loading by digital image correlation. The intelligent hybrid method proposed by Nishioka et al. was applied to the stress-strain analysis near the crack tip. The accuracy of stress-intensity factor at the free surface was discussed from the viewpoint of both the experiment and 3-D finite element analysis. The surface images before and after deformation were taken by a CMOS camera, and we developed the system which enabled the real time stress analysis based on digital image correlation and inverse problem analysis. The great portion of processing time of this system was spent on displacement analysis. Then, we tried improvement in speed of this portion. In the case of cracked body, it is also possible to evaluate fracture mechanics parameters such as the J integral, the strain energy release rate, and the stress-intensity factor of mixed-mode. The 9-points elliptic paraboloid approximation could not analyze the displacement of submicron order with high accuracy. The analysis accuracy of displacement was improved considerably by introducing the Newton-Raphson method in consideration of deformation of a subset. The stress-intensity factor was evaluated with high accuracy of less than 1% of the error.

***Keywords*—**Digital Image Correlation, Mixed Mode, Newton -Raphson Method, Stress Intensity Factor.

## I. Introduction

WHEN a structure was superannuated conventionally, newly remaking was almost the case. However, the industrial filed in the world has the idea in use of using it for a long time, by evaluating and diagnosing the soundness of a structure and repairing it selectively from fields, such as profitability, a resource, an environment, and energy. Although various sensors are developed for soundness assessment (health monitoring) of a structure in order to evaluate a stress and a strain quantitatively in a certain territory of an actual structure, there are many troubles which should be conquered, such as cost, time, and a labor. An actual structure is 3-D and opaque in many cases, and internal 3-D displacement and stress measurement are considerably difficult. Then, the stress and the strain in the surface have been measured mainly. Industrially, most strain gages are used. However, since it is point measurement, in order to carry out full field measurement in a certain territory, it needs many gages, an apparatus, and time.

In this study, the hybrid stress-analysis method which enables the stress and the strain analyses from the experimental information on the surface obtained with digital image correlation method [1]-[6] was developed. Since the displacement data obtained from the experiment includes the error of measurement, it is almost impossible to analyze the stress and the strain from raw displacement data. Then, the intelligent hybrid method [7]-[9] which corrects the error of the experimental displacement data and makes a stress analysis possible was applied [10]-[12]. In order to build the system which combined digital image correlation method, and the 9-points elliptic paraboloid approximation and the intelligent hybrid method and to evaluate the availability of the system, the stress analysis of the acrylic specimen with a crack subjected to mixed-mode loading was conducted. The stress intensity factor of the mixed mode obtained from this has about 10 % of error, and sufficient accuracy was not acquired. Moreover, since it became clear that deformation of a subset must be taken into consideration from the result, the system which newly combined digital image correlation method using the Newton-Raphson method (NRM) [2], [3], [5] and the intelligent hybrid method was built. In order to evaluate the availability of this system, the mode I load was applied to the aluminum specimen with a crack, and the comparison with the 3-D finite element method (FEM) was performed. By this system, it became clear that the stress intensity factor is evaluated with high accuracy.

## II. Principles

### A. Digital Image Correlation

2-D digital image correlation allows the measurement of full-field, in-plane displacement from digital images before and after deformation. Two digital images of A $\{x_i=1, 2, \ldots.., N\}$ and B $\{y_i=1, 2, \ldots\ldots, N\}$ were taken before and after loading. The correlation coefficient $\rho$ is calculated by

$$\rho = \frac{\frac{1}{N}\sum_{i=1}^{N}(x_i-\bar{x})(y_i-\bar{y})}{s_x s_y} \quad (1)$$

where $s_x$, $s_y$ are standard deviations of image A and image B, respectively, $x_i$ and $y_i$ are the averages of the gray level of

Manuscript received March 15, 2006. This work was supported by Grant-in-Aid for scientific Research of Japan Society for the Promotion of Science, No.16560079. We are grateful for the support.

K. Machida is with Tokyo University of Science, Noda-shi, Chiba, 278-8510 Japan (phone: +81-4-7122-9597; fax: +81-4-7123-9814; e-mail: mac@rs.noda.tus.ac.jp).

H. Yamada was a graduate student with Tokyo University of Science, Noda-shi, Chiba, 278-8510 Japan. He is now with Denso Corporation, Kariya, Aichi, 448-8661, Japan (e-mail: hyamada@rlab.denso.co.jp).

images. As $\rho$ is higher, it can be said these two subsets resemble each other. Although the information on a pixel is 4 bytes in colour, since analyses are possible enough with gray level values, only the intensity is used. Most digital image correlation algorithms work by searching the gray value pattern in small local neighborhoods commonly referred to as a subset. A similarity measure is employed to determine the displacement of the subset center in a second image (under loading).

In the intelligent hybrid method, since the mesh by 8-nodes isoparametric element is adopted, the measuring points are first arranged so that they may correspond to the nodes of the mesh. Next, in order to measure displacement of each node, a certain territory (subset) is cut out from the image before deformation centering on a node. In order to calculate to which location of the image the subset moved after deformation, a correlation coefficient is calculated as a table of $3\times3$. The nine-points are taken focusing on the highest point in the table, and this process is continued until the center takes the highest correlation coefficient. It is considered that the location converged eventually is a result of coarse search. Only the movement magnitude in a pixel unit can be found in this phase. Therefore, many methods are developed to calculate sub-pixel order deformation. In these methods, we chose the nine-point elliptic paraboloid approximation by the least-squares method. Elliptic paraboloid shown in Fig. 1 is expressed by (2).

$$Z = 1 - \rho = \frac{(x-c)^2}{a^2} + \frac{(y-d)^2}{b^2} \tag{2}$$

In this approximation, we can find the correct point of the displacement which is the lowest point in the surface.

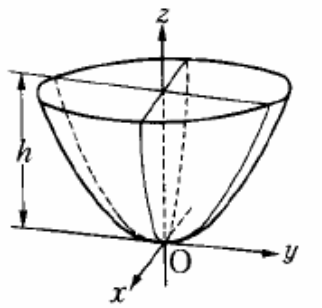


Fig. 1 Elliptic paraboloid

### *B. Newton-Raphson Method*

Although the subset before deformation uses a rectangle in actual displacement analysis, since the image after deformation is transforming itself, we have to take this into consideration. Then, the deformation term of the subset is defined as follows as $P_i$.

$$P_i = \{u, v, \frac{\partial u}{\partial x}, \frac{\partial u}{\partial y}, \frac{\partial v}{\partial x}, \frac{\partial v}{\partial y}\} \tag{3}$$

If the coordinates after deformation of the point in this subset (x, y) are made into (x*, y*), (x*, y*) can be expressed by the following equations.

$$\begin{aligned} x^* &= x + u + \frac{\partial u}{\partial x}\Delta x + \frac{\partial u}{\partial y}\Delta y \\ y^* &= y + v + \frac{\partial v}{\partial x}\Delta x + \frac{\partial v}{\partial y}\Delta y \end{aligned} \tag{4}$$

where $\Delta x$ and $\Delta y$ are the distances from a subset center to point ($x$, $y$), respectively. The coordinates ($x^*$, $y^*$) after deformation are not an integer overwhelmingly in many cases. Then, the gray level values between pixels after deformation were interpolated with the Lagrange interpolating polynomial of 3-th degree. The Newton-Raphson method is applied to these six deformation parameters.

$$\Delta P_i = -H^{-1} * \nabla P_i \tag{5}$$

The Hessian matrix $H$ and the Jacobian matrix $\nabla P_i$ in (5) are expressed by the following equations.

$$H = \begin{bmatrix} \frac{\partial^2\rho}{\partial u\partial u} & \frac{\partial^2\rho}{\partial u\partial v} & \frac{\partial^2\rho}{\partial u\partial\left(\frac{\partial u}{\partial x}\right)} & \frac{\partial^2\rho}{\partial u\partial\left(\frac{\partial u}{\partial y}\right)} & \frac{\partial^2\rho}{\partial u\partial\left(\frac{\partial v}{\partial x}\right)} & \frac{\partial^2\rho}{\partial u\partial\left(\frac{\partial v}{\partial y}\right)} \\ \frac{\partial^2\rho}{\partial v\partial u} & \frac{\partial^2\rho}{\partial v\partial v} & \frac{\partial^2\rho}{\partial v\partial\left(\frac{\partial u}{\partial x}\right)} & \frac{\partial^2\rho}{\partial v\partial\left(\frac{\partial u}{\partial y}\right)} & \frac{\partial^2\rho}{\partial v\partial\left(\frac{\partial v}{\partial x}\right)} & \frac{\partial^2\rho}{\partial v\partial\left(\frac{\partial v}{\partial y}\right)} \\ \frac{\partial^2\rho}{\partial\left(\frac{\partial u}{\partial x}\right)\partial u} & \frac{\partial^2\rho}{\partial\left(\frac{\partial u}{\partial x}\right)\partial v} & \frac{\partial^2\rho}{\partial\left(\frac{\partial u}{\partial x}\right)\partial\left(\frac{\partial u}{\partial x}\right)} & \frac{\partial^2\rho}{\partial\left(\frac{\partial u}{\partial x}\right)\partial\left(\frac{\partial u}{\partial y}\right)} & \frac{\partial^2\rho}{\partial\left(\frac{\partial u}{\partial x}\right)\partial\left(\frac{\partial v}{\partial x}\right)} & \frac{\partial^2\rho}{\partial\left(\frac{\partial u}{\partial x}\right)\partial\left(\frac{\partial v}{\partial y}\right)} \\ \frac{\partial^2\rho}{\partial\left(\frac{\partial u}{\partial y}\right)\partial u} & \frac{\partial^2\rho}{\partial\left(\frac{\partial u}{\partial y}\right)\partial v} & \frac{\partial^2\rho}{\partial\left(\frac{\partial u}{\partial y}\right)\partial\left(\frac{\partial u}{\partial x}\right)} & \frac{\partial^2\rho}{\partial\left(\frac{\partial u}{\partial y}\right)\partial\left(\frac{\partial u}{\partial y}\right)} & \frac{\partial^2\rho}{\partial\left(\frac{\partial u}{\partial y}\right)\partial\left(\frac{\partial v}{\partial x}\right)} & \frac{\partial^2\rho}{\partial\left(\frac{\partial u}{\partial y}\right)\partial\left(\frac{\partial v}{\partial y}\right)} \\ \frac{\partial^2\rho}{\partial\left(\frac{\partial v}{\partial x}\right)\partial u} & \frac{\partial^2\rho}{\partial\left(\frac{\partial v}{\partial x}\right)\partial v} & \frac{\partial^2\rho}{\partial\left(\frac{\partial v}{\partial x}\right)\partial\left(\frac{\partial u}{\partial x}\right)} & \frac{\partial^2\rho}{\partial\left(\frac{\partial v}{\partial x}\right)\partial\left(\frac{\partial u}{\partial y}\right)} & \frac{\partial^2\rho}{\partial\left(\frac{\partial v}{\partial x}\right)\partial\left(\frac{\partial v}{\partial x}\right)} & \frac{\partial^2\rho}{\partial\left(\frac{\partial v}{\partial x}\right)\partial\left(\frac{\partial v}{\partial y}\right)} \\ \frac{\partial^2\rho}{\partial\left(\frac{\partial v}{\partial y}\right)\partial u} & \frac{\partial^2\rho}{\partial\left(\frac{\partial v}{\partial y}\right)\partial v} & \frac{\partial^2\rho}{\partial\left(\frac{\partial v}{\partial y}\right)\partial\left(\frac{\partial u}{\partial x}\right)} & \frac{\partial^2\rho}{\partial\left(\frac{\partial v}{\partial y}\right)\partial\left(\frac{\partial u}{\partial y}\right)} & \frac{\partial^2\rho}{\partial\left(\frac{\partial v}{\partial y}\right)\partial\left(\frac{\partial v}{\partial x}\right)} & \frac{\partial^2\rho}{\partial\left(\frac{\partial v}{\partial y}\right)\partial\left(\frac{\partial v}{\partial y}\right)} \end{bmatrix} \tag{6}$$

$$\nabla P_i = \begin{Bmatrix} \frac{\partial\rho}{\partial u} \\ \frac{\partial\rho}{\partial v} \\ \frac{\partial\rho}{\partial\left(\frac{\partial u}{\partial x}\right)} \\ \frac{\partial\rho}{\partial\left(\frac{\partial u}{\partial y}\right)} \\ \frac{\partial\rho}{\partial\left(\frac{\partial v}{\partial x}\right)} \\ \frac{\partial\rho}{\partial\left(\frac{\partial v}{\partial y}\right)} \end{Bmatrix} \tag{7}$$

The partial corrections are calculated using (5). $P_{i+1}$ after performing i+1 time calculation can be obtained from the following recurrence equation.

$$P_{i+1} = P_i + \Delta P_i \tag{8}$$

This process is iterated until convergence is obtained.

### *C. Intelligent Hybrid Method*

The 2-D intelligent hybrid method proposed by Nishioka

et al. was employed to evaluate the stress and the strain using equation. displacement data. The intelligent hybrid method is formulized based on a variational principle which minimizes an experimental error. The variational principle is expressed as

$$\int_V \sigma_{ij}^{\mathrm{mod}}\,\delta\varepsilon_{ij}^{\mathrm{mod}}\,dV = \int_{S_t} \bar{t}_i \delta u_i^{\mathrm{mod}}\,dS + \int_V \bar{f}_i \delta u_i^{\mathrm{mod}}\,dV - \int_V \sigma_{ij}^{\mathrm{exp}}\,\delta\varepsilon_{ij}^{\mathrm{mod}}\,dV \tag{9}$$

where $V$ is the hybrid analysis area. $S$ means a boundary of the hybrid analysis area. $\sigma_{ij}^{\mathrm{exp}}$ is the stress obtained by the experiment. $u_i^{\mathrm{mod}}$, $\sigma_{ij}^{\mathrm{mod}}$ and $\varepsilon_{ij}^{\mathrm{mod}}$ are the displacement, the stress and the strain in the modifying field. $\bar{t}_i$ and $\bar{f}_i$ are traction and body forces, respectively. The hybrid analysis area is divided into some regions, and equation (9) is expressed by vector notation as

$$\sum_n \int_{V_n} \{\sigma^{\mathrm{mod}}\}^T \{\delta\varepsilon^{\mathrm{mod}}\}\,dV = \sum_n \left[ \int_{S_{tn}} \{\bar{t}\}^T \{\delta u^{\mathrm{mod}}\}\,dS + \int_{V_n} \{\bar{f}\}^T \{\delta u^{\mathrm{mod}}\}\,dV - \int_{V_n} \{\sigma^{\mathrm{exp}}\}^T \{\delta\varepsilon^{\mathrm{mod}}\}\,dV \right] \tag{10}$$

where $n$ is the element number, $V_n$ and $S_{tn}$ are the region and mechanical boundary of the $n$-th element, respectively. The displacement vector in the element is expressed as follows

$$\{u\} = \{u^{\mathrm{exp}}\} + \{u^{\mathrm{mod}}\} = [N](\{q^{\mathrm{exp}}\} + \{q^{\mathrm{mod}}\}) \tag{11}$$

where $[N]$ denotes the shape function matrix, $\{q^{mod}\}$ and $\{q^{exp}\}$ are the nodal displacement vectors of the modifying and experimental fields in the element, respectively. The stress and the strain are similarly expressed by the following equation:

$$\{\varepsilon\} = \{\varepsilon^{\mathrm{exp}}\} + \{\varepsilon^{\mathrm{mod}}\} = [B](\{q^{\mathrm{exp}}\} + \{q^{\mathrm{mod}}\}) \tag{12}$$

$$\{\sigma\} = \{\sigma^{\mathrm{exp}}\} + \{\sigma^{\mathrm{mod}}\} = [D][B](\{q^{\mathrm{exp}}\} + \{q^{\mathrm{mod}}\}) \tag{13}$$

where $[B]$ and $[D]$ are strain-displacement and elastic coefficient matrices, respectively.

From (10)-(13), one obtains the following finite element equation:

$$[K]\{Q^{\mathrm{mod}}\} = \{F\} - [K]\{Q^{\mathrm{exp}}\} \tag{14}$$

where $\{Q^{mod}\}$ and $\{Q^{exp}\}$ are the nodal displacement vectors of the modifying and experimental fields in the entire hybrid analysis region, respectively. $[K]$ and $\{F\}$ are the global stiffness matrix and the global nodal force vectors, respectively. Usually, the experimental displacement field contains measurement errors so that the right-hand side of (14) is not zero.

$$\{R\} = \{F\} - [K]\{Q^{\mathrm{exp}}\} \neq 0 \tag{15}$$

where $\{R\}$ is the restoration force vectors. The modifying displacement field can be evaluated by solving the following

$$[K]\{Q^{\mathrm{mod}}\} = \{R\} \tag{16}$$

$\{Q^{mod}\}$ can be obtained from the 2-D FEM by putting $R$ as the nodal load and constraining all nodes at the outer boundary in the x and y directions. Since the analysis accuracy is influenced by smoothing of the displacement on the outer boundary, we need to pay attention enough to smoothing [10]. Finally, the true displacement field is obtained by the following equation.

$$\{Q\} = \{Q^{\mathrm{exp}}\} + \{Q^{\mathrm{mod}}\} \tag{17}$$

Thus, obtained displacement filed $u_i$ ($=u_i^{\mathrm{exp}} + u_i^{\mathrm{mod}}$) by the intelligent hybrid method satisfies the principle of minimum potential energy and the principle of virtual work, as well as the equilibrium equation.

If an appropriate displacement filed can be obtained, from the following equation, the strain can be evaluated from the displacement of each node, and the stress can be evaluated from the strain.

$$\{\varepsilon\} = [B]\{\delta\}^e \tag{18}$$

$$\{\sigma\} = [D]\{\varepsilon\} \tag{19}$$

where $\{\delta\}^{\mathrm{e}}$ is the nodal displacement vectors of an element.

## III. Experiment and FEM Model

The acrylic resin has a low Young's modulus and greatly deforms. Although an image is captured with low magnification, since deformation can be checked, it is advantageous when calculating with pixel unit. Then, we employed the acrylic resin as the material of the specimen. Young's modulus and Poisson's ratio of acrylic resin were 3.06 GPa and 0.38, respectively. The specimen configuration is shown in Fig. 2. $\alpha$ in the figure is a load application angle. The mixed-mode loading was applied to the specimen using a device proposed by Richard and Benitz [13] as shown in Fig. 3. This device enables us to carry out the experiments under seven kinds of mixed-mode loading. The degree of load application angle was changed by a unit of 15 degrees from 0 to 90 degrees, and the images before and after deformation were taken with the CMOS camera. Then, the intelligent hybrid method proposed by Nishioka et al. was applied to the stress-strain analysis. Consequently, the stress and the strain near the crack tip can be evaluated with high accuracy. The stress-intensity factors $K_I$ and $K_{II}$ were evaluated by the virtual crack extension method [14][15].

To simplify the comparison between stress-intensity factors ($K_I$, $K_{II}$), the non-dimensional stress-intensity factors ($F_I$, $F_{II}$) were evaluated as follows:

$$F_j = \frac{K_j}{\frac{P}{WB}\sqrt{\pi a}} \qquad (j = I, II) \tag{20}$$

Here, $P$ is the load, $W$ and $B$ are the width and thickness of the specimen, respectively, and $a$ is a crack length.

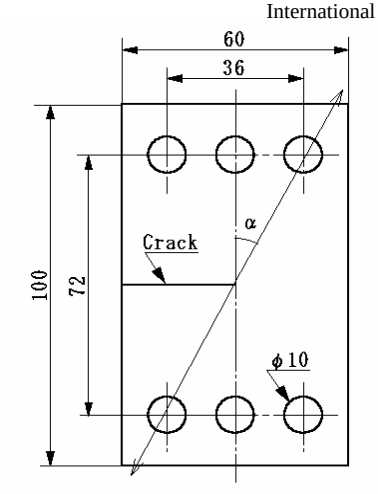


Fig. 2 Specimen configuration

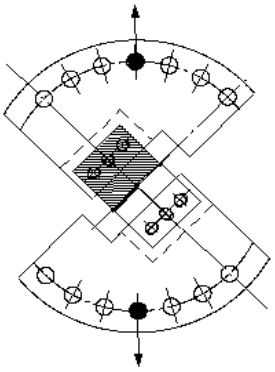

Fig. 3 Mixed-mode device

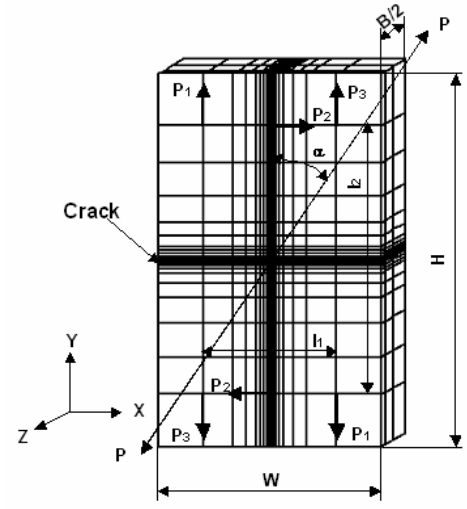


Fig. 4 3-D mesh of FEM

Accuracy assessment was performed from the comparison with the result of 3-D FEM and the experimental result obtained by the 9-points elliptic paraboloid approximation and the intelligent hybrid method.

The 3-D mesh of FEM is shown in Fig. 4. Next, the need for algorithm of taking deformation into consideration to pattern matching has been recognized from the analyses as the result of the above-mentioned mixed mode experiment. Then, the new system which combined the Newton-Raphson method which took deformation of the subset into consideration, and the intelligent hybrid method was developed. In order to evaluate this system, the experiment under mode I loading was conducted using the compact tension specimen of aluminum alloy A2017-T3. The specimen configuration is shown in Fig. 5. Young's modulus, Poisson's ratio and the yield stress are 70.3 GPa, 0.33 and 304 MPa, respectively. Fig. 6 shows the 3-D mesh of FEM.

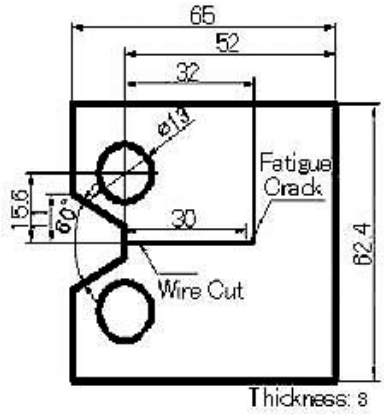


Fig. 5 Specimen configuration

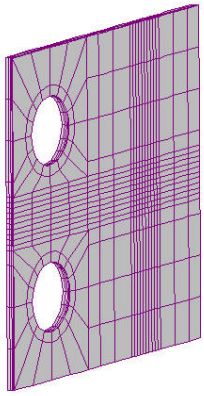

Fig. 6 3-D mesh of FEM

## IV. Results And Discussions

As the example of mixed mode loading, the images of $\alpha$=45 degrees used for displacement measurement are shown in Fig. 7. The size of this image is 500 [W] × 500 [H] pixels, magnification is 0.00425 mm/pixel, and the loads before and after loading are 21.0 N and 200.0 N, respectively.

Fig. 8 shows the distribution of displacement obtained by the 9-points elliptic paraboloid approximation. A remarkable difference is shown in the x-direction displacement between FEM and the intelligent hybrid method. The amount of deformation which straddles a crack of the intelligent hybrid method is smaller than that of FEM. This originates in that there are few absolute values of deformation. It is theoretically difficult to calculate the amount of displacement of the sub-pixel in digital image correlation method. When analyzing especially actual deformation, a subset is extracted before deformation, but it is searched for where it moved after deformation. However, in order for the subset itself to change, accuracy falls. In the case of this analysis, it is completely in the range of the sub-pixel which is less than 0.5 pixel at the point of largest displacement. As a result, it seems that a good result was not obtained since correlation was not able to be taken well.

Next, although a good result is generally obtained, the displacement in the y direction is greatly dented in the upper

and the lower parts at the crack tip. There is a line of a longitudinal direction near the crack tip as shown in Fig. 7, but this is considered to be the cause of error. That is, the image which has a line perpendicularly is unsuitable to vertical displacement analyses, and considering a principle, we can understand this easily. The contour map of stress in the y direction in $\alpha$=45 degrees is shown in Fig. 9. Although the good result is obtained near the crack, big turbulence can be seen near the outer boundary. Since the intelligent hybrid method constrains the outer boundary and calculates, the error of small displacement of the outer boundary causes a big stress concentration. This is a theoretic problem and needs to examine the method which will correct this error from now on.

The variation of the non-dimensional stress intensity factor with a load application angle is shown in Fig. 10. Although there are a few points exceeding 10 %, the difference between both is less than 10 % at almost all angles. The absolute value of the difference is small and does not pose a big problem. The stress intensity factor obtained by both methods was in agreement in general.

Although a mixed mode load is added to a test piece by the six pins of the upper and the lower sides, the holes of the both ends of loading device are the long circles to a transverse direction and the central holes are the long circles to a longitudinal direction, so that the contact condition with the holes of loading device and the pins varies delicately with the load application angle. Therefore, since the constraint conditions of FEM and experiment were not strictly in agreement, it is thought that the error arose. Although it was able to obtain the stress intensity factor with less than 10% of the error mostly by the old experiment approach, if deformation is taken into consideration, it will be thought that accuracy is raised more.

Although the accuracy of the intelligent hybrid method is greatly influenced by the accuracy of the outer boundary of the analysis region, since the outer boundary of the analysis region is distant from the crack tip, its deformation is large and its error is large by an old approach. Since the actual deformation is not a rectangle and the subset itself deforms, it is considered that the analysis accuracy of the sub-pixel improves by taking this into consideration. Then, the experimental result using the Newton-Raphson method in consideration of deformation is shown below.

The images actually used for analyses are shown in Fig. 11. The magnitude of an image is 500 [W] × 500 [H] pixels, and the magnification is 0.02378 mm/pixel. The loads before and after deformation are 102.0 N and 499.5 N, respectively. The distribution of the displacement obtained by the Newton Raphson method is shown in Fig. 12. At the crack opening part of the left-hand side of the image, it is seen that the displacement in the x direction is slightly curving on left-hand side. It is considered that it is because the algorithm cannot respond to deformation of the subset completely. In this location, since the subset is close to a trapezoid, it is thought that such an error has come out.

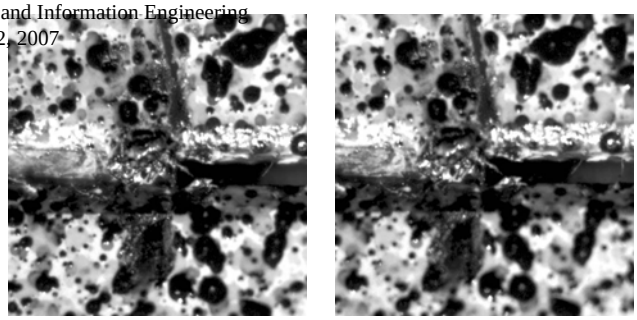

(a) Before deformation (b) After deformation

Fig. 7 Images of the displacement analysis

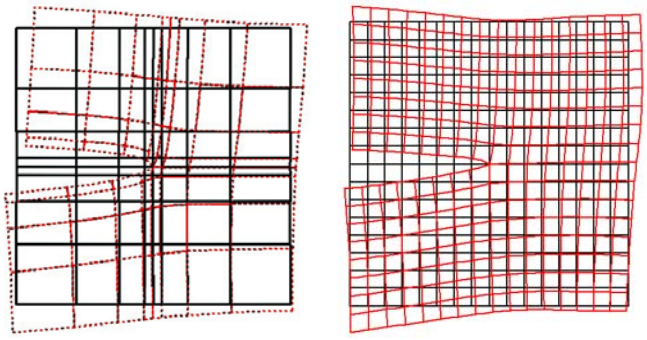

(a) Result of FEM (b) Result of hybrid method

Fig. 8 Displacement distribution by 9-points elliptic paraboloid approximation

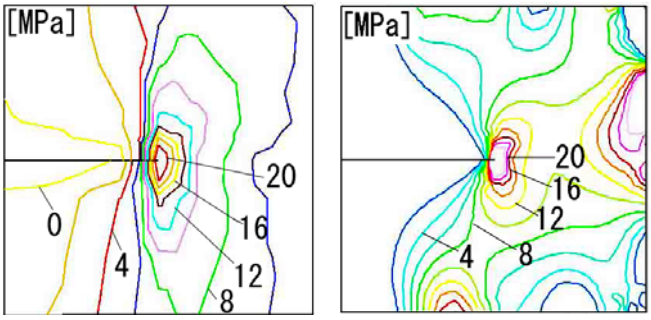


(a) Result of FEM (b) Result of hybrid method

Fig. 9 Contour map of $\sigma_y$ in $\alpha$=45 degrees

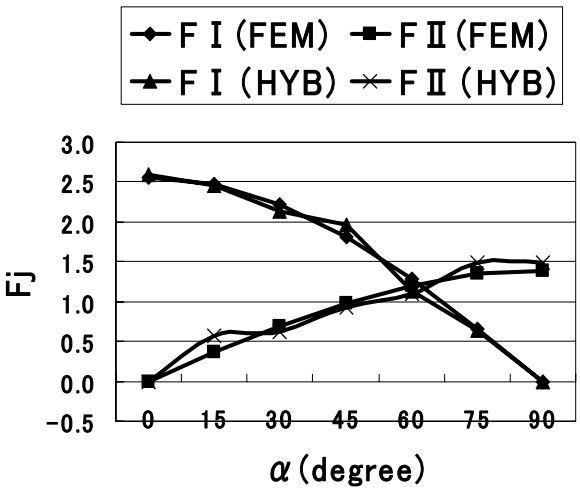


Fig. 10 Variation of non-dimensional stress intensity factors with a load application angle

The contour map of $\sigma_y$ is shown in Fig. 13. First, if its attention is paid to the outer boundary, although turbulence has arisen like Fig. 9, the result whose distribution configuration is quite good is obtained. Although a thing like a big stress concentration can be seen at the upper part and the lower part of left-hand side, this is caused by the result in displacement analyses.

About a crack problem, there is a stress intensity factor as a standard which evaluates analysis accuracy synthetically.

Finally, this stress intensity factor is compared. As seen in Table I, as for the result of the Newton-Raphson method, the result better than the 9-points elliptic paraboloid approximation is obtained. Although the relative error with the result of FEM was quite as large as 6.4 % in the 9-points elliptic paraboloid approximation, the very good result was obtained with 0.8 % and less than 1 % of an error in the Newton-Raphson method. Also in the experimental result of other cases, 0.5 % of the error and the good result are obtained, and the effectiveness of this method was verified.

TABLE I
NON-DIMENSIONAL STRESS INTENSITY FACTOR $F_I$

| Method | 3-dimensional Finite Element Method | Newton-Raphson Method | 9-points Elliptic Palaboloid Approximation |
|---|---|---|---|
| S.I.F. | 11.048 | 11.132 | 10.336 |

## V. CONCLUSION

(1) The system using digital image correlation method, and the 9-points elliptic paraboloid approximation and the intelligent hybrid method enabled it to evaluate a mixed mode stress intensity factor by less than 10 % of error.

(2) By introducing the algorithm in consideration of the deformation using the Newton-Raphson method, the accuracy of displacement analyses was considerably improved.

(3) The system using digital image correlation method, the Newton-Raphson method, and the intelligent hybrid method enabled it to evaluate a stress intensity factor by less than 1 % of error.

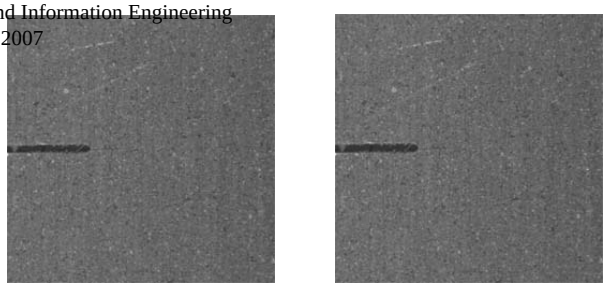

(a) Before deformation (b) After deformation

Fig. 11 Images for displacement analysis

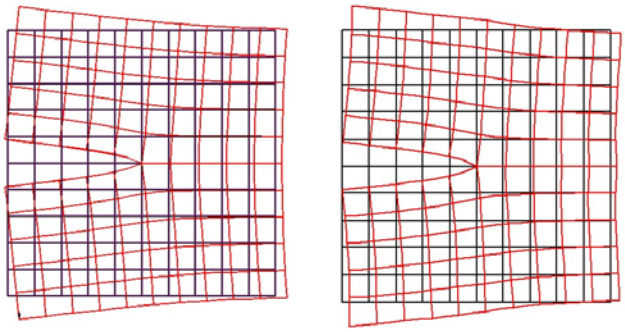

(a) Result of FEM (b) Result of hybrid method

Fig. 12 Displacement distribution

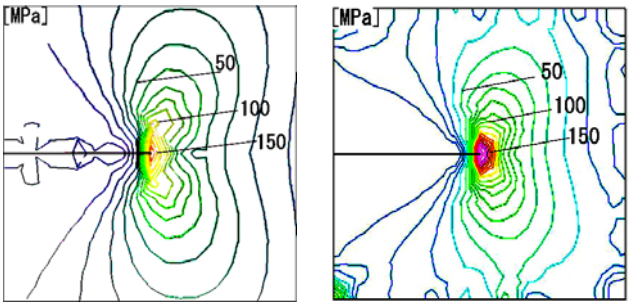


(a) Result of FEM (b) Result of hybrid method

Fig. 13 Contour map of $\sigma_y$

## REFERENCES

[1] M. A. Sutton, M. Chenng, W. H. Peters, Y. J. Chao & S. R. McNeill, "Application of an optimized digital correlation method to planar deformation analysis, image and vision computing," vol. 4-3, 1986, pp. 143-150.

[2] H. A. Bruck, S. A. McNeill, M. A. Sutton and W. H. III Peter, "Digital image correlation using Newton-Raphson method of partial differential correction," *Exp. Mech*., vol. 29-3, 1989, pp. 261-268.

[3] G. Vendroux & W. G. Knauss, "Submicron deformation field measurements: Part2. Improved digital image correlation," *Exp. Mech*., vol. 38, 1998, pp. 86-92.

[4] M. A. Sutton, S. R. McNeill, J. D. Helm & Y. Chao, "Advances in two-dimensional and 3-D computer vision," In *Photomechanics*, P. K. Rastagi, Ed., Germany, Springer-Verlag, 2000, pp. 323-372.

[5] C. Su and L. Anand, "A new digital image correlation algorithm for whole-field displacement measurement," *IMST Symp*. 2003, 2003, 8 pages.

[6] I. Nishikawa and S. Abe, "Development of RGB digital image correlation method using Lagrange interpolation," *Proc. JSEM* (in Japanese), No.4-2, 2004, pp. 278-281
T. Nishioka, H. Ikekita and K. Tamai, "A variational principle for minimizing experimental measurement errors and its application to a hybrid experimental-numerical method," *Comp. Mech*., vol. 20, 1997, pp. 101-108.

[7] T. Nishioka, K. Kurio and H. Nakabayashi, "An intelligent hybrid method to automatically detected and eliminate experimental measurement errors for linear elastic deformation fields," *Exp. Mech*., vol. 40-2, 2000, pp. 170-179.

[8] T. Nishioka, T. Fujimoto and R. Nishioka, "Measurement of the Near Field of an Interface of Crack Tip by the Intelligent Hybrid Method," *Trans. JSME* (in Japanese), vol. 67-655A, 2001, pp. 424-431.

[9] K. Machida, K. Usui and H. Okamura, "Stress analysis near crack tip in mixed-mode condition by speckle photography using an intelligent hybrid method, Advances in fracture research," *Proc. ICF10*, ELSEVIER, CD-ROM-edition, 2001, 6 pages.

[10] K. Machida and K. Usui, "Stress analysis inside the specimen under mixed-mode loading by hybrid speckle photography," *Trans. JSME* (in Japanese), vol. 68-676A, 2002, pp. 1794-1800.

[11] K. Machida, "Stress analysis inside the specimen under mixed-mode loading by 3-D hybrid method," *Advance in Comp. & Exp. Eng. and Sci.*, CD-ROM-edition, 2003, 6 pages.

[12] H. A. Richard and K. Benitz, "A loading device for the creation of mixed mode in fracture mechanics," *Intl. J. Fract*., vol. 22, 1983, pp. R55-R58.

[13] D. M. Parks, "A stiffness derivative finite element technique for determination of elastic crack tip stress intensity factors," *Intl. J. Fract*., vol. 10, 1974, pp. 487-502.

[14] K. Machida, "Stress intensity factors of a mixed-mode interface crack by a finite element analysis," *Trans. JSME* (in Japanese), vol. 62-599A, 1996, pp. 1565-1570.